Advances in Nano Research, *Vol. 16, No. 1 (2024) 11-26*
https://doi.org/10.12989/anr.2024.16.1.011

Free vibration analysis of FG porous spherical cap reinforced by graphene platelet resting on Winkler foundation

Xiangqian Shen*[1], Tong Li[1], Lei Xu[1], Faraz Kiarasi[2], Masoud Babaei**[2] and Kamran Asemi[3]

[1]*XiHua University, Chengdu 610039, China*
[2]*Department of Mechanical Engineering, University of Eyvanekey, Eyvanekey, Semnan, Iran,*
[3]*Department of Mechanical Engineering, Islamic Azad University, North Tehran Branch, Tehran, Iran*

(*Received December 11, 2022, Revised October 26, 2023, Accepted October 30, 2023*)

Abstract. In this study, free vibration analysis of FG porous spherical cap reinforced by graphene platelets resting on Winkler-type elastic foundation has been surveyed for the first time. Three different types of porosity patterns are considered for the spherical cap whose two types of porosity patterns in the metal matrix are symmetric and the other one is uniform. Besides, five GPL patterns are assumed for dispersing of GPLs in the metal matrix. Tsai-Halpin and extended rule of the mixture are used to determine the Young modulus and mass density of the shell, respectively. Employing 3D FEM elasticity in conjunction with Hamilton's Principle, the governing motion equations of the structure are obtained and solved. The impact of various parameters including porosity coefficient, various porosity distributions in conjunction with different GPL patterns, the weight fraction of graphene Nano fillers, polar angles and stiffness coefficient of elastic foundation on natural frequencies of FG porous spherical cap reinforced by GPLs have been reported for the first time.
Keywords: FEM; functionally graded porous; graphene platelets; spherical cap; natural frequency; Winkler elastic foundation; 3D elasticity

1. Introduction

Shell-type structures, in particular spherical shells, are extensively applied in aerospace, marine and submarine industries. The natural frequency analysis will be important to prevent from resonance in these applications. Therefore, many investigations have been performed on the free vibration analysis of shell-type structures made of isotropic, composite and functionally graded materials (FGMs) (Al-Furjan *et al*. 2022a, b, Al-Osta 2021, Bouafia *et al*. 2021, Bot *et al*. 2022, Cuong-Le *et al*. 2022, Faghidian and Tounsi 2022, Hadji *et al*. 2023, Katiyar *et al*. 2022, Kong *et al*. 2022, Liu *et al*. 2022, Rouabhia *et al*. 2020, Van Vinh and Tounsi 2022a, b). Among them, spherical shells have received less attention by researchers. In detail, Du (*et al*. 2019) presented a unified formulation for the free vibration of a spherical cap based on first-order shear deformation theory (FSDT) and employing Ritz method. Khinchi and Sharma (2020) applied COMSOL as commercial software to investigate natural frequencies of isotropic- and FG-spherical caps with cutouts by considering clamped-clamped and free-free boundary conditions. Gautham and Ganesan (1992) presented a semi-analytical solution for free vibration analysis of thick spherical shells with and without center cutout based on thick shell theory. Du (*et al*. 2019) studied the natural frequencies of spherical cap subjected to different boundary conditions based on thin shell theory and the Ritz method. Gao (*et al*. 2020) applied FSDT to present an approximate solution for vibrations of uniform and stepped FG spherical cap based on Ritz method. Artioli and Voila (2006) investigated the natural frequencies of spherical caps based on FSDT and using generalized differential quadrature method (GDQM). Ram and Ram and Babu (2002) performed an investigation about free vibration of composite spherical shell cap with and without a cutout by using the finite element method (FEM) based on a higher-order shear deformation theory (HSDT). Free vibration characteristics of FG porous spherical shell with general boundary conditions by using FSDT and Ritz approach was presented by Li *et al*. (2019) Barzegar and Fadaee and Fadaee (2018) introduced a decoupling analytical approach for vibration analysis of FG spherical caps subjected to thermal load based on FSDT. Thi Phuong *et al*. (2020) used Galerkin method to study the nonlinear vibration of FG sandwich spherical caps resting on elastic foundations by applying FSDT in a thermal environment. Pang *et al*. (2019) presented a semi-analytical solution by applying Rayleigh–Ritz method for free vibration of FG spherical shell based on FSDT. Based on FSDT and by utilizing Ritz approach, an accurate unified solution for vibration analysis of arbitrary functionally graded spherical shell segments with general end restraints was presented by Su *et al*. (2014). By employing FEM based HSDT, free vibration of functionally graded carbon nanotube reinforced composite spherical shell cap was presented by Susmith and Ram (2019). Natural frequency of thick FGM spherical shells with all edges clamped or simply supported based on a third-order shear deformation theory was presented by Zannon *et al*. (2020). Mirjavandi *et al*. (2021) investigated

*Corresponding author, Assistant Professor,
E-mail: shenxiangqian121@sina.com
**Corresponding author, Assistant Professor,
E-mail: Masoudbabaei@eyc.ac.ir

ISSN: 2287-237X (Print), 2287-2388 (Online)

geometrically nonlinear vibration analysis of eccentrically stiffened porous functionally graded annular spherical shell segments based on thin shell theory in conjunction with von Karman–Donnell sense and by applying smeared stiffeners method. Ye *et al*. (2014) applied 3D elasticity theory based on Rayleigh–Ritz approach to investigate the vibration analysis of laminated FG spherical shells with general boundary conditions. Asadzadeh and Eslami (2018) investigated the vibrations of an FGM spherical cap subjected to thermal load based on FSDT and applied Ritz procedure. Using a 3 noded axisymmetric curved shell element based on the field consistency approach, vibrations and thermal stability of FG spherical caps were presented by Prakash *et al*. (2006). Quang Minh *et al*. (2022) studied nonlinear axisymmetric vibration of sandwich FGM spherical caps with lightweight porous core based on FSDT in conjunction with von Kármán geometrical nonlinearity and by utilizing Galerkin approach and the Runge–Kutta procedure. Flis and Muc (2021) presented an analytical solution for FG porous spherical shell of revolution based on the Love–Kirchhoff hypothesis. Due to the importance of vibration of spherical shell structures, reviews on vibration analysis of FGM spherical shell were performed by Khinchi and Sharma (2019) and Punera and Kant (2019).

Nowadays, there is a high demand for lightweight structures widely applied in many industries, especially aerospace. Because of the lightweight and relatively high strength, porous material has been applied in various spacecraft parts in the aerospace industry. In recent years, scientists have continuously tried to identify new materials that have high performance, but also they are increasing the performance of previous materials by combining them with nanoparticles and fabricating metallic or polymeric nanocomposite. Among nanoparticles, graphene platelets (GPLs) have revealed substantial abilities to choose a proper reinforcement candidate due to they have excellent mechanical properties with lower fabricating cost, larger specific surface area and 2-D geometry. Therefore, researchers have done many investigations on the behavior of the structures, such as those made of FG porous material reinforced by GPLs and multilayer GPL reinforced composites (Al-Furjan *et al*. 2021). There are many researches on the behavior of these structures subjected to various loading, including static, dynamic, buckling and thermal, the researchers related to the vibration of shell structures are mentioned here. For instance, Safarpour *et al*. (2020) investigated the static and free vibration analysis of FG-GPL truncated conical shells, cylindrical shells and annular plates with various boundary conditions based on 3D elasticity theory. Bahaadini *et al*. (2019) presented an analytical solution for the natural frequency of FG-GPL porous truncated conical shell based on Love's first approximation theory. Ye and Wang (2021) employed Galerkin method to study the internal resonance of FG-GPL-reinforced metal foam cylindrical shells based on Donnell's nonlinear shell theory. Based on improved Donnell nonlinear shell theory, Wang *et al*. (2019) performed an investigation about the nonlinear vibration of metal foam cylindrical shells reinforced with GPLs by employing Galerkin approach. Moradi Dastjerdi and Behdinan (2021) presented a meshless solution based on an axisymmetric model and moving least squares (MLSs) interpolation functions for stress waves in thick porous graphene-reinforced cylinders subjected to thermal gradient environments. An analytical solution for nonlinear vibration of shear deformable imperfect FG-GPL porous nano-composite cylindrical shells based on FSDT was presented by Salehi *et al*. (2021). Nejadi *et al*. (2021) presented a GDQM solution as semi analytical formulation for free vibration of sandwich cylindrical shell based on FSDT and by considering porosity and GPL effects on conveying fluid flow. Zhou *et al*. (2021) studied vibration and flutter characteristics of GPL-reinforced functionally graded porous cylindrical panels under supersonic flow based on Reddy's TSDT and by applying the standard Lagrange procedure. Ton-That *et al*. (2021) investigated the nonlinear forced vibration of FG-GPL-reinforced metal foam cylindrical shells based on Donnell's nonlinear shell theory and by applying Galerkin method. Ebrahimi *et al*. (2019) presented an analytical solution for free vibration analysis of FG porous shells reinforced by GPLs based on the FSDT. Pourjabari *et al*. (2019) presented an analytical method for free and forced vibration characteristics of the GPL reinforcement composite cylindrical shell based on modified strain gradient theory (MSGT). An analytical solution for vibration analysis of FG porous truncated conical shells reinforced by GPLs based on Love's first approximation theory was reported by Bahaadini *et al*. (2019). Kiarasi *et al*. (2021) employed FEM based on Rayleigh- Ritz method and 2D elasticity theory to study the free vibration analysis of FG porous joined truncated conical –cylindrical shell reinforced by GPLs. Babaei *et al*. (2021) performed an investigation about natural frequency and stress wave propagation analyses of FG porous joined truncated conical –cylindrical-conical shells by employing 2D elasticity theory in conjunction with FEM based Rayleigh- Ritz method and Newmark procedure.

Despite the available literature mentioned above, however, it seems that dynamic behavior of FG-GPL porous spherical shells have not been surveyed so far. Also, literature review denotes that the free vibration response of spherical cap shells has not been independently investigated even for porous or GPL-reinforced ones. Besides, most of the investigations on the vibration analysis of spherical shells are based on shell theories. Hence, Due to the potential of these structures in practical aerospace and marine applications, it is necessary to study the behavior of spherical caps made of a FG-GPL porous material, with a particular attention to their free vibration response, because of their large exposure to dynamic loads. This aspect is, thus, explored in the present work, and the motion equilibrium equations are determined using the theory of linear three-dimensional elasticity, and Hamilton's Principle, whose solution is found according to classical finite elements. Applying 3D FEM elasticity rather than shell theories provides more accurate results due to considering thickness sketching.

The spherical cap of present study features a uniform and non-uniform pattern of GPLs in the metallic matrix including open-cell internal pores and three various porosity

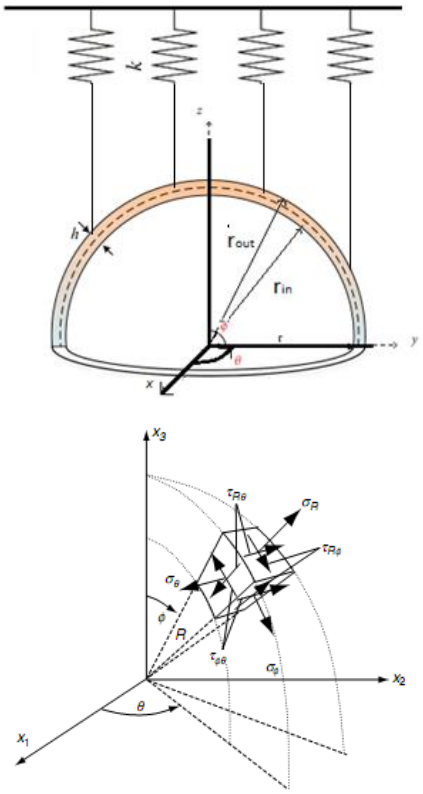

Fig. 1 Coordinate system, geometric parameters and stress components of a spherical cap

distributions across the shell thickness with uniform and symmetric FG patterns. In addition, five different patterns of GPL dispersion pattern are assumed through the shell thickness, namely, a FG GPL-X, A, V, UD and O pattern. A systematic investigation checks for the effect of various porosity distributions and GPL patterns, as well as the porosity coefficients and weight fractions of nano-fillers and different polar angles, on the free vibration of FG porous spherical caps reinforced by GPLs.

2. Theoretical formulations

2.1 Description of the Geometry:

Assume a spherical cap made of uniform thickness h, and mean radius R. The outer and inner radii of the spherical cap are indicated by R_{out}=b and R_{in}=a, respectively. The spherical cap is referred to the spherical coordinates r, $0 \le \theta \le 2\pi$ and $0 \le \varphi \le \pi$ which are respectively radial direction, azimuthal angle in x-y plane and polar angle, as shown in Fig. 1.

2.2 Estimating mechanical properties of the spherical cap:

Three different porosity distributions are assumed through the spherical cap thickness (Fig. 2). Two types of non-uniform symmetric porosity distributions and a uniform porosity distribution are considered. In distribution 1, the porosity is symmetric, nonlinear, and its distribution around the mid-radius is higher than its distribution around the inner and outer surfaces of the spherical cap. In distribution 2, the porosity is also symmetric and nonlinear, but the porosity near the inner and outer surfaces of the spherical cap is higher than that around the mid-radius. The distribution of material properties considering the effect of porosity for distributions 1, 2 and 3 are given in Eqs (1), (2) and (3), respectively. Besides, three GPL distribution patterns along the spherical cap thickness are indicated in Fig. 2 and given in Eq. (15) (Kitipornchai *et al*. 2017 and Yang *et al*. 2018).

The mechanical properties including Young's modulus E(r), shear modulus G(r) and mass density ρ(r)of porous nanocomposite spherical cap are described as follows (Zhou *et al*. 2019, Arshid *et al*. 2021, Bekkaye *et al*. 2020, Bellifa *et al*. 2021, Guellil *et al*. 2021, Kumar *et al*. 2021 and Van Vinh *et al*. 2022):

Porosity distribution 1 (Non-uniform symmetric I):

$$\begin{cases} E(r) = E^*\left[1 - e_0\cos\left(\pi(\frac{r-r_{in}}{h} - \frac{1}{2})\right)\right] \\ G(r) = G^*\left[1 - e_0\cos\left(\pi(\frac{r-r_{in}}{h} - \frac{1}{2})\right)\right] \\ \rho(r) = \rho^*\left[1 - e_m\cos\left(\pi(\frac{r-r_{in}}{h} - \frac{1}{2})\right)\right] \end{cases} \quad (1)$$

Porosity distribution 2 (Non-uniform symmetric II):

$$\begin{cases} E(r) = E^*\left[\left(1 - e_0^*(1\text{-}\cos\left(\pi(\frac{r-r_{in}}{h} - \frac{1}{2})\right)\right)\right] \\ G(r) = G^*\left[\left(1 - e_0^*(1\text{-}\cos\left(\pi(\frac{r-r_{in}}{h} - \frac{1}{2})\right)\right)\right] \\ \rho(r) = \rho^*\left[\left(1 - e_m^*(1\text{-}\cos\left(\pi(\frac{r-r_{in}}{h} - \frac{1}{2})\right)\right)\right] \end{cases} \quad (2)$$

Uniform porosity distribution:

$$\begin{cases} E(\varsigma) = E^*\alpha \\ G(\varsigma) = G^*\alpha \\ \rho(\varsigma) = \rho^*\alpha' \end{cases} \quad (3)$$

where $E*, G*$ and $\rho*$ being the Young's modulus, shear modulus and mass density of GPL spherical cap without interior cavities, respectively. Also, e_0 and e_0^* ($0 \le e_0(e_0^*) < 1$) introduce the coefficients of porosity for distributions 1 and 2, respectively. $e_m$and e_m^*indicate the mass density coefficient for distributions 1 and 2, respectively. α and α' are the parameters of uniform porosity distribution. As the size and density of interior cavities increase, the porosity increases, and consequently, causes a reduction in the material properties. The relation between Young modulus and density for open-cell metal foams is presented in Eq. (4) (Ansari *et al*. 2021, Yaghoobi and Taheri 2020).

$$\frac{E(r)}{E^*} = \left(\frac{\rho(r)}{\rho^*}\right)^2 \quad (4)$$

Eq. (4) is utilized to derive the relation between the porosity coefficients and mass density coefficients for various porosity patterns as follows:

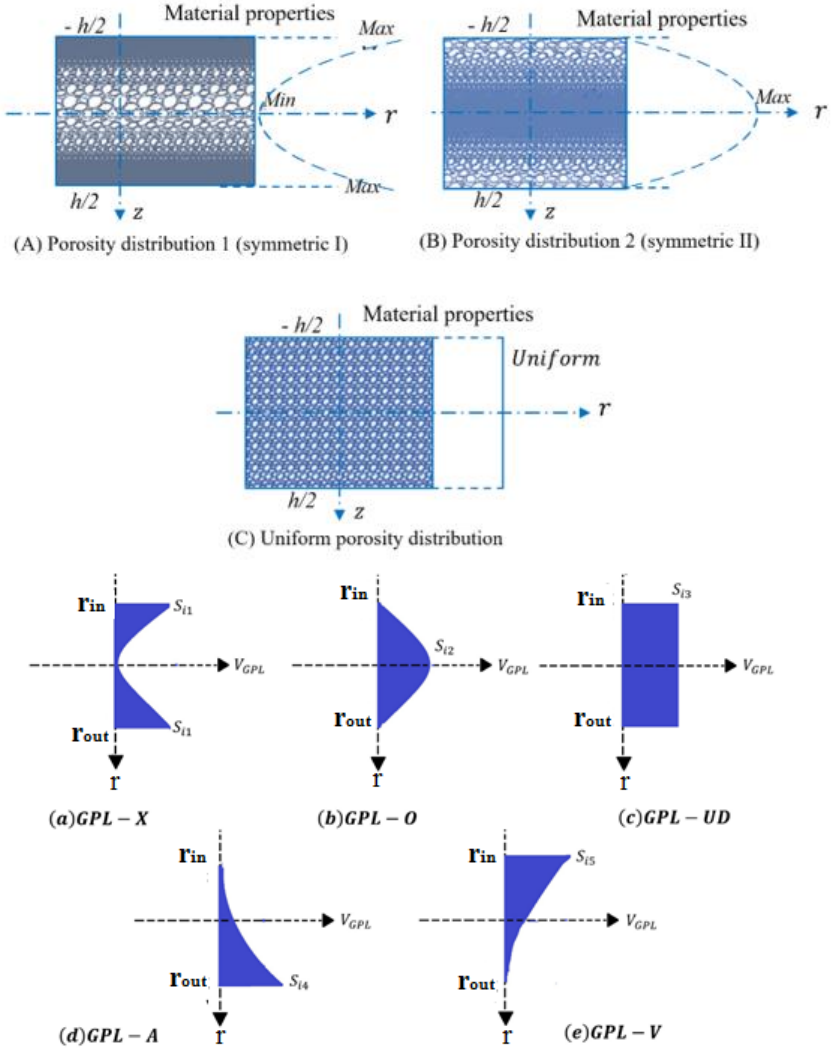

Fig. 2 Patterns of Porosity and GPL distributions

$$\begin{cases} 1-e_m\cos(\pi \mathrm{r}) = \sqrt{1-e_0 cos(\pi \mathrm{r})} \\ 1-e_m^*(1-cos(\pi \mathrm{r})) = \sqrt{1-e_0^*(1-cos(\pi \mathrm{r}))} \\ \alpha' = \sqrt{\alpha} \end{cases} \quad (5)$$

Here, it is assumed that the mass of various spherical caps with various porosity patterns and GPL dispersions are identical.

$$\int_{rin}^{rout} \sqrt{1-e_0\cos(\pi \mathrm{r})}\ \mathrm{dr} = \int_{rin}^{rout} \sqrt{1-e_0^*(1-cos(\pi \mathrm{r}))}d\mathrm{r} = \int_0^{h/2} \sqrt{\alpha}\mathrm{dr} \quad (6)$$

According to Eq (6), the values of e_0^* and α can be estimated with a known value of e_0, as given in Table 1. It is seen that e_0^* increases as e_0 increases. When e_0 is 0.6, e_0^* is calculated to be 0.9612 which is near to the upper bound. Thus, $e_0 \in [0, 0.6]$ is used in this work.

According to Halpin-Tsai micromechanics model (Tao and Dai 2021, Heidari *et al*. 2021 and Nguyen *et al*. 2020), the Young's modulus of the nanocomposite without interior cavities is expressed as:

$$E^* = \frac{3}{8}\left(\frac{1+\varepsilon_L^{GPL}\eta_L^{GPL}V_{GPL}}{1-\eta_L^{GPL}V_{GPL}}\right)E_m + \frac{5}{8}\left(\frac{1+\varepsilon_W^{GPL}\eta_W^{GPL}V_{GPL}}{1-\eta_W^{GPL}V_{GPL}}\right) \quad (7)$$

$$\varepsilon_L^{GPL} = \frac{2l_{GPL}}{t_{GPL}} \quad (8)$$

$$\varepsilon_W^{GPL} = \frac{2w_{GPL}}{t_{GPL}} \quad (9)$$

$$\eta_L^{GPL} = \frac{E_{GPL}-E_m}{E_{GPL}+\varepsilon_L^{GPL}E_m} \quad (10)$$

$$\eta_W^{GPL} = \frac{E_{GPL}-E_m}{E_{GPL}+\varepsilon_W^{GPL}E_m} \quad (11)$$

where indices m and GPL denote the properties of the metallic matrix and graphene platelets, respectively. V_{GPL}

is the volume content of GPLs and l_{GPL}, w_{GPL} and t_{GPL} are, respectively, length, width and thickness of nanofiller platelets.

Employing the rule of mixture, the mass density and Poisson's ratio of the nanocomposite are estimated as follows (Tao and Dai 2021, Huang *et al*. 2021, Mangalasseri *et al*. 2023 and Nguyen *et al*. 2020):

$$\rho^* = \rho_{GPL}V_{GPL} + \rho_m(1 - V_{GPL}) \tag{12}$$

$$v^* = v_{GPL}V_{GPL} + v_m(1 - V_{GPL}) \tag{13}$$

The $G*$ shear modulus of the nanocomposite expresses as bellow:

$$G^* = \frac{E^*}{2(1+v^*)} \tag{14}$$

The volume content of GPLs, V_{GPL}, is assumed to change across the spherical cap thickness with five dispersion patterns as follows (see also Fig. (2)):

$$V_{GPL}(r) = \begin{Bmatrix} S_{i1}[1 - cos\left(\pi(\frac{r-r_{in}}{h} - \frac{1}{2})\right)]GPL - X \\ S_{i2}c\,os\left(\pi(\frac{r-r_{in}}{h} - \frac{1}{2})\right)GPL - O \\ S_{i3}GPL - UD \\ S_{i4}[1 - cos(\pi(\frac{r-r_{in}}{2h})]GPL - A \\ S_{i5}\,cos(\pi(\frac{r-r_{in}}{2h})GPL - V \end{Bmatrix} \tag{15}$$

where $S_{i1}, S_{i2}, S_{i3}, S_{i4}$ and S_{i5} denote the upper limit of the V_{GPL}, and subscript i =1, 2 and 3 denote various porosity distributions 1, 2, 3 within each pattern. V_{GPL}^T is the total volume content of GPL and is estimated by applying the nanofiller weight fraction Δ_{GPL} into Eq.(16), then it is used to derive S_{i1}, S_{i2}, S_{i3}, S_{i4} and S_{i5} by Eq. (17) .

$$V_{GPL}^T = \frac{\Delta_{GPL}\rho_m}{\Delta_{GPL}\rho_m + \rho_{GPL} - \Delta_{GPL}\rho_{GPL}} \tag{16}$$

$$V_{GPL}^T \int_{r_{in}}^{r_{out}} \frac{\rho(r)}{\rho^*} dr = \begin{Bmatrix} S_{i1}\int_{r_{in}}^{r_{out}} [1 - cos\left(\pi(\frac{r-r_{in}}{h} - \frac{1}{2})\right)]\frac{\rho(r)}{\rho^*}dr \\ S_{i2}\int_{r_{in}}^{r_{out}} c\,os\left(\pi(\frac{r-r_{in}}{h} - \frac{1}{2})\right)\frac{\rho(r)}{\rho^*}dr \\ S_{i3}\int_{r_{in}}^{r_{out}} \frac{\rho(r)}{\rho^*}dr \\ S_{i4}\int_{r_{in}}^{r_{out}} [1 - cos(\pi(\frac{r-r_{in}}{2h})]\frac{\rho(r)}{\rho^*}dr \\ S_{i5}\int_{r_{in}}^{r_{out}} cos(\pi(\frac{r-r_{in}}{2h})\frac{\rho(r)}{\rho^*}dr \end{Bmatrix} \tag{17}$$

2.2 Governing Equations

Neglecting body forces, the equations of motion in spherical coordinates are obtained as (Sadd 2009):

$$\begin{aligned} &\frac{\partial \sigma_r}{\partial r} + \frac{1}{r}\frac{\partial \sigma_{r\phi}}{\partial \phi} + \frac{1}{r\sin\phi}\frac{\partial \sigma_{r\phi}}{\partial \theta} + \\ &\frac{1}{r}\left(2\sigma_r - \sigma_\theta - \sigma_\phi + \sigma_{r\phi}\cot\phi\right) = \rho^*(r)\frac{\partial^2 u}{\partial t^2} \\ &\frac{\partial \sigma_{r\theta}}{\partial r} + \frac{1}{r}\frac{\partial \sigma_\phi}{\partial \phi} + \frac{1}{r\sin\phi}\frac{\partial \sigma_{\theta\phi}}{\partial \theta} + \\ &\frac{1}{r}\left(\sigma_\phi - \sigma_\theta\right)\cot\phi + 3\sigma_{r\phi} = \rho^*(r)\frac{\partial^2 v}{\partial t^2} \\ &\frac{\partial \sigma_{r\theta}}{\partial r} + \frac{1}{r}\frac{\partial \sigma_{\theta\phi}}{\partial \phi} + \frac{1}{r\sin\phi}\frac{\partial \sigma_\theta}{\partial \theta} + \\ &\frac{1}{r}\left(2\sigma_{\theta\phi}\cot\phi + 3\sigma_{r\theta}\right) = \rho^*(r)\frac{\partial^2 w}{\partial t^2} \end{aligned} \tag{18}$$

where *u*, *v* and *w* are the displacement components along the r,φ and θ directions, respectively and $\rho^*(r)$ is the mass density that depends on r coordinates.

The stress-strain relations from the Hook's law in the matrix form are as:

$$\sigma = D\varepsilon \tag{19}$$

where the stress and strain components and the coefficients of elasticity D, are as the following relations:

$$\sigma = \{\sigma_r \quad \sigma_\phi \quad \sigma_\theta \quad \sigma_{r\phi} \quad \sigma_{\theta\phi} \quad \sigma_{r\theta}\}^T \tag{20}$$

$$\varepsilon = \{\varepsilon_r \quad \varepsilon_\phi \quad \varepsilon_\theta \quad \gamma_{r\phi} \quad \gamma_{\phi\theta} \quad \gamma_{r\theta}\}^T \tag{21}$$

$$D = \frac{E^*(r)}{(1+v^*)(1-2v^*)} \begin{bmatrix} 1-v^* & v^* & v^* & 0 & 0 & 0 \\ v^* & 1-v^* & v^* & 0 & 0 & 0 \\ v & v & 1-v^* & 0 & 0 & 0 \\ 0 & 0 & 0 & \frac{1-2v^*}{2} & 0 & 0 \\ 0 & 0 & 0 & 0 & \frac{1-2v^*}{2} & 0 \\ 0 & 0 & 0 & 0 & 0 & \frac{1-2v^*}{2} \end{bmatrix} \tag{22}$$

where v^* denotes the Poisson's ratio and E^* is the Young's modulus of elasticity that depends on r coordinate.

The strain-displacement equations based on the theory of linear elasticity in spherical coordinate are:

$$\begin{aligned} \varepsilon_r &= \frac{\partial u}{\partial r}, \quad \varepsilon_\phi = \frac{1}{r}\left(u + \frac{\partial v}{\partial \phi}\right) \\ \gamma_{\theta\phi} &= \frac{1}{2r}\left(\frac{1}{\sin\phi}\frac{\partial v}{\partial \theta} + \frac{\partial w}{\partial \phi} - \cot\phi\, w\right) \\ \gamma_{r\phi} &= \frac{1}{2}\left(\frac{1}{r}\frac{\partial u}{\partial \phi} + \frac{\partial v}{\partial r} - \frac{v}{r}\right) \\ \varepsilon_\theta &= \frac{1}{r\sin\phi}\left(\frac{\partial w}{\partial \theta} + \sin\phi\, u + \cos\phi\, v\right) \\ \gamma_{r\theta} &= \frac{1}{2}\left(\frac{1}{r\sin\phi}\frac{\partial u}{\partial \theta} + \frac{\partial w}{\partial r} - \frac{w}{r}\right) \end{aligned} \tag{23}$$

and in the matrix form are as:

$$\varepsilon = \mathcal{L}U \tag{24}$$

where **U** is the displacements vector and $\mathcal{L}$ is a matrix containing partial differentiating equations as:

$$U = \{u \quad v \quad w\}^T \tag{25}$$

$$\mathcal{L} = \begin{bmatrix} \partial_r & 1/r & 1/r & 1/2r\,\partial_\phi & 0 & \frac{1}{2r\sin\phi}\partial_\theta \\ 0 & 1/r\,\partial_\phi & 1/r\,\cot\phi & \frac{1}{2}\partial_r - \frac{1}{2r} & \frac{1}{2r\sin\phi}\partial_\theta & 0 \\ 0 & 0 & \frac{1}{r\sin\phi}\partial_\theta & 0 & \partial_\phi - \cot\phi & \partial_r - \frac{1}{r} \end{bmatrix}^T \tag{26}$$

The clamped boundary conditions are defined as:

For a spherical cap with θ=180˚, φ=180˚:
u, v, w (r, θ, φ=0, 180˚)

For a spherical cap with θ=180˚, φ=90˚:
u, v, w (r, θ, φ=0, 90˚) (27)

2.3 Graded finite element modeling

In order to solve the governing equations, the graded finite element method is used. Applying the graded elements for modeling of gradation of the material leads to more accurate results than dividing the solution domain into homogenous elements. The spherical cap is divided into a number of 8–node linear elements. For element (e), the displacements in three directions are approximated as follow:

$$U^{(e)} = \Phi \Lambda^{(e)} \tag{28}$$

where Φ is the matrix of linear shape functions in cylindrical coordinate and $\Lambda^{(e)}$ is the nodal displacement vector of the element that are as:

$$\Phi = \begin{bmatrix} \Phi_1 & 0 & 0 & \cdots & \Phi_8 & 0 & 0 \\ 0 & \Phi_1 & 0 & \cdots & 0 & \Phi_8 & 0 \\ 0 & 0 & \Phi_1 & \cdots & 0 & 0 & \Phi_8 \end{bmatrix} \tag{29}$$

$$\Lambda^{(e)} = \{U_1 \quad V_1 \quad W_1 \quad \cdots \quad U_8 \quad V_8 \quad W_8\}^T \tag{30}$$

The components of Φ are:

$$\Phi_i = \frac{1}{V} \Gamma X \tag{31}$$

where V is the volume of each element that is:

$$V = \begin{vmatrix} 1 & \xi_1 & \eta_1 & \zeta_1 & \xi_1\eta_1 & \xi_1\zeta_1 & \eta_1\zeta_1 & \xi_1\eta_1\zeta_1 \\ 1 & \xi_2 & \eta_2 & \zeta_2 & \xi_2\eta_2 & \xi_2\zeta_2 & \eta_2\zeta_2 & \xi_2\eta_2\zeta_2 \\ 1 & \xi_3 & \eta_3 & \zeta_3 & \xi_3\eta_3 & \xi_3\zeta_3 & \eta_3\zeta_3 & \xi_3\eta_3\zeta_3 \\ 1 & \xi_4 & \eta_4 & \zeta_4 & \xi_4\eta_4 & \xi_4\zeta_4 & \eta_4\zeta_4 & \xi_4\eta_4\zeta_4 \\ 1 & \xi_5 & \eta_5 & \zeta_5 & \xi_5\eta_5 & \xi_5\zeta_5 & \eta_5\zeta_5 & \xi_5\eta_5\zeta_5 \\ 1 & \xi_6 & \eta_6 & \zeta_6 & \xi_6\eta_6 & \xi_6\zeta_6 & \eta_6\zeta_6 & \xi_6\eta_6\zeta_6 \\ 1 & \xi_7 & \eta_7 & \zeta_7 & \xi_7\eta_7 & \xi_7\zeta_7 & \eta_7\zeta_7 & \xi_7\eta_7\zeta_7 \\ 1 & \xi_8 & \eta_8 & \zeta_8 & \xi_8\eta_8 & \xi_8\zeta_8 & \eta_8\zeta_8 & \xi_8\eta_8\zeta_8 \end{vmatrix} \tag{32}$$

and:

$$\Gamma_{ij} = (-1)^{i+j} \left| A_{ij} \right| \tag{33}$$

$$X = \{1, \xi, \eta, \zeta, \xi\eta, \xi\zeta, \eta\zeta, \xi\eta\zeta\}^T \tag{34}$$

in which:

$$\xi = r\cos\theta\sin\phi, \quad \eta = r\sin\theta\sin\phi, \quad \zeta = r\cos\phi \tag{35}$$

$$\xi_i = r_i\cos\theta_i\sin\phi_i, \quad \eta_i = r_i\sin\theta_i\sin\phi_i, \quad \zeta_i = r_i\cos\phi_i \tag{36}$$

where r_i , θ_i and ϕ_i are nodal coordinates and A_{ij} is obtained from eliminating i^{th} row and j^{th} column of V.

To treat the material inhomogeneity by using the GFEM, it may be written:

$$\Psi^{(e)} = \sum_{i=1}^{8} \Psi_i \Phi_i \tag{37}$$

where $\psi(e)$ is the material property of the element.

Substituting Eq. (28) in Eq. (24) gives the strain matrix of element (e) as:

$$\varepsilon^{(e)} = B\Lambda^{(e)} \tag{38}$$

where:

$$B = \mathcal{L}\Phi^{(e)} \tag{39}$$

Now by using Hamilton's principle and Rayleigh-Ritz energy formulation, the GFEM is imposed and finally mass and stiffness matrices are obtained as followingrelations:

$$\int_{t_1}^{t_2} \delta(\Pi - \mathrm{T})dt = 0 \tag{40}$$

where Π , T are potential energy, kinetic energy, respectively. These functions and their variations are:

$$\Pi = \frac{1}{2}\iiint_V \varepsilon^T \sigma dV \tag{41}$$

$$\delta\Pi = \iiint_V \delta\varepsilon^T \sigma dV \tag{42}$$

$$T = \frac{1}{2}\iiint_V \rho\dot{U}^T\dot{U}dV \tag{43}$$

$$\delta T = \iiint_V \rho\dot{U}^T\delta\dot{U}dV \tag{44}$$

where V and A are the volume and area of the domain.

Substituting Eqs. (41)-(44) in Hamilton's Principle, applying side conditions $\delta U|_{t_1,t_2} = 0$ and using part integration:

$$\iiint_V \delta\varepsilon^T \boldsymbol{\sigma} dV + \left(\iint_A K_W\, u\, \delta u\, dA \right)_{r=b} + \iiint_V \rho\ddot{\boldsymbol{U}}^T \delta\boldsymbol{U} dV = 0 \tag{45}$$

$$dV = r^2 \sin\phi\, dr\, d\phi\, d\theta,\ dA = r^2 \sin\phi\, d\phi\, d\theta$$

The second term in the above equation is the potential

energy of Winkler elastic foundation which is exerted to outer surface of spherical cap. Also, for each element, by imposing Eqs. (19), (28) and (38) into Eq. (45), it can be achieved:

$$\delta\Lambda^{(e)^T}\left\{\iiint_V \rho\Phi^T\Phi dV\right\}\ddot{\Lambda}^{(e)} + \delta\Lambda^{(e)^T}\left\{\iiint_V B^T DBdV\right\}\Lambda^{(e)} + \delta\Lambda^{(e)^T}\left(\int \overline{N}^T K_w \overline{N} dA\right)_{r=b}\Lambda^{(e)} = 0$$

$$\overline{N} = \begin{bmatrix} 0 & 0 & 0 & 0 & 0 & 0 & 0 & 0 & 0 & 0 & 0 & 0 & N_5 & 0 & 0 & N_6 & 0 & 0 & N_7 & 0 & 0 & N_8 & 0 & 0 \\ 0 & 0 & 0 & 0 & 0 & 0 & 0 & 0 & 0 & 0 & 0 & 0 & 0 & 0 & 0 & 0 & 0 & 0 & 0 & 0 & 0 & 0 & 0 & 0 \\ 0 & 0 & 0 & 0 & 0 & 0 & 0 & 0 & 0 & 0 & 0 & 0 & 0 & 0 & 0 & 0 & 0 & 0 & 0 & 0 & 0 & 0 & 0 & 0 \end{bmatrix} \quad (46)$$

In the first row of $\overline{N}$ which is for shape functions of u, only the shape functions of outer face of element that are subjected to elastic foundation are considered. Now by assembling the element matrices, the global equations of motion for FG porous spherical cap reinforced by graphene platelet can be written as:

$$[M]\left\{\ddot{\Lambda}\right\} + [K + K_w]\{\Lambda\} = 0 (47) \quad (47)$$

Solving the system of eigenvalue in Eq. (47), the natural frequencies and mode shapes are obtained.

$$([K + K_w] - [M]\omega^2)\{\Lambda\} = 0 \quad (48)$$

where the characteristic matrices are defined as:

$$M^{(e)} = \iiint_V \rho\Phi^T\Phi dV \quad (49)$$

$$K^{(e)} = \iiint_V B^T \boldsymbol{DB} dV \quad (50)$$

$$K_w = \int \overline{N}^T K_w \overline{N} dA \quad (51)$$

3. Numerical results and discussion

In this section, the results of natural frequencies of FG-GPL porous spherical cap with clamped boundary conditions for various volume weight fractions of GPL, GPL distribution pattern, porosity distribution and porosity coefficient as well as two polar angles of FG porous spherical shell reinforced by graphene platelet are investigated.

3.1 Validation

To verify the results obtained in this study, the present study is validated by ANSYS WORKBENCH as commercial software for natural frequencies of isotropic homogeneous spherical caps. Hence the following changes should be considered in our MATLAB CODE.

$$e_0 = 0, \gamma_{GPL} = 0$$

Mechanical property: E_m=130GPa, ρ_m = 8960 kg/m^3, υ_m = 0.34 for copper

Geometry: a=0.225 m, b=0.25 m, θ=180˚,$\varphi = 180^0, 90^0$

By this way, the FG GPL porous structure changes to homogenous structure.

The comparison between the present result and ANSYS WORKBENCH is shown in Table 2. This comparison shows an excellent agreement between them.

3.2 Natural frequencies of FG porous spherical cap reinforced by GPLs

In this section, the influence of two polar angles, porosity coefficient and porosity distribution, GPL patterns and weight fraction of GPL nanofillers on natural frequencies of a FG-GPL porous spherical cap with clamped boundaries have been reported for the first time. Hence, the following material properties and geometrical parameters are considered:

Geometry: a=0.225 m, b=0.25 m, θ=180˚,$\varphi = 180^0, 90^0$

Material property: E_m 130GPa, ρ_m 8960 kg/m3, υ_m 0.34 for copper (Kiarasi *et al*. 2021), and E_{GPL} 1.01 TPa, ρ_{GPL} 1062.5 kg/m^3, υ_{GPL}, w_{GPL} 1.5 μm, l_{GPL} 2.5 μm, t_{GPL} 1.5 nm for GPLs.

Table 3 shows the effect of two types of polar angles and various GPL patterns on the natural frequencies of FG porous spherical reinforced by GPLs (PD1, e_0=0.4, $\gamma = 0.01wt\%$). The maximum and minimum values of fundamental natural frequencies are related to GPLX and GPL-V, respectively. It means that when GPLs are more concentrated around the inner and outer surface of shell, the shell has it maximum stiffness and vibrates with higher natural frequencies. Also, when the GPLs are more dispersed around the outer surface of shell, the shell stiffness of shell is lower than other GPL distributions and minimum natural frequencies are obtained. It is mentioned that the amount of fundamental natural frequencies of GPLO, A and GPL-UD is approximately the same. This point is very important for the designers, and they can use these distributions instead of each other. Also, results show that by increasing the polar angle, the surface area of shell increases and subsequently, the bending stiffness and the natural frequency decreases. The same results and conclusions are obtained and shown in Tables 4 and 5 for PD2 and PD3, respectively (e_0=0.4, $\gamma = 0.01wt\%$). A comparison between results of Table 3 and 5 shows that the maximum and minimum fundamental natural frequencies for FG-A,V,UD and O distributions belong to PD3 and PD2, respectively. The effect of two polar angles and various porosity distributions are reported in Table 6 for GPLX distribution (e_0=0.2,$\gamma = 0.01wt\%$). The maximum and minimum fundamental natural frequencies belong to PD1 and PD2, respectively. On the other hand, PD1 provides more rigidity for the structure, while PD2 gives the

Table 2 Comparison of natural frequencies between present study and ANSYS WORKBENCH

Polar angle		ω_1	ω_2	ω_3	ω_4	ω_5	ω_6
180°	(ANSYS WORKBENCH)	1412.7	1472.9	2147.7	2387.2	2488.1	2720.3
	(Present)	1401.3	1458.6	2107.7	2370.1	2450.8	2690.8
90°	(ANSYS WORKBENCH)	2710	2921.3	2971.9	3634.1	3652.3	3691.5
	(Present)	2701	2901.8	2913.8	3600.8	3620.9	3618.6

Table 3 Natural frequencies (Hz) of FG-GPL porous spherical cap for various polar angles and GPL patterns (PD1, e_0=0.4,$\gamma = 0.01wt\%$)

GPL pattern	φ	ω_1	ω_2	ω_3	ω_4	ω_5	ω_6
GPL-X	180^0	2251.6	2251.7	3196.2	3690.7	3691.5	4203.1
	90^0	3880.5	4257.1	4289.6	5274.9	5338.2	5439.8
GPL-A	180^0	1847.9	1848.3	2608.1	3002.4	3003.3	3389.2
	90^0	3145.0	3391.5	3449.5	4219.7	4239.4	4286.5
GPL-V	180^0	1669.6	1669.9	2357.0	2713.1	2714.0	3062.0
	90^0	2841.2	3062.1	3115.9	3809.0	3829.3	3869.2
GPL-O	180^0	1803.8	1804.2	2536.3	2916.5	2917.5	3267.9
	90^0	3045.2	3231.6	3315.8	3994.0	4042.4	4066.6
GPL-UD	180^0	1849.7	1850.0	2610.6	3005.2	3006.0	3392.4
	90^0	3147.2	3392.7	3451.4	4220.5	4241.7	4287.1

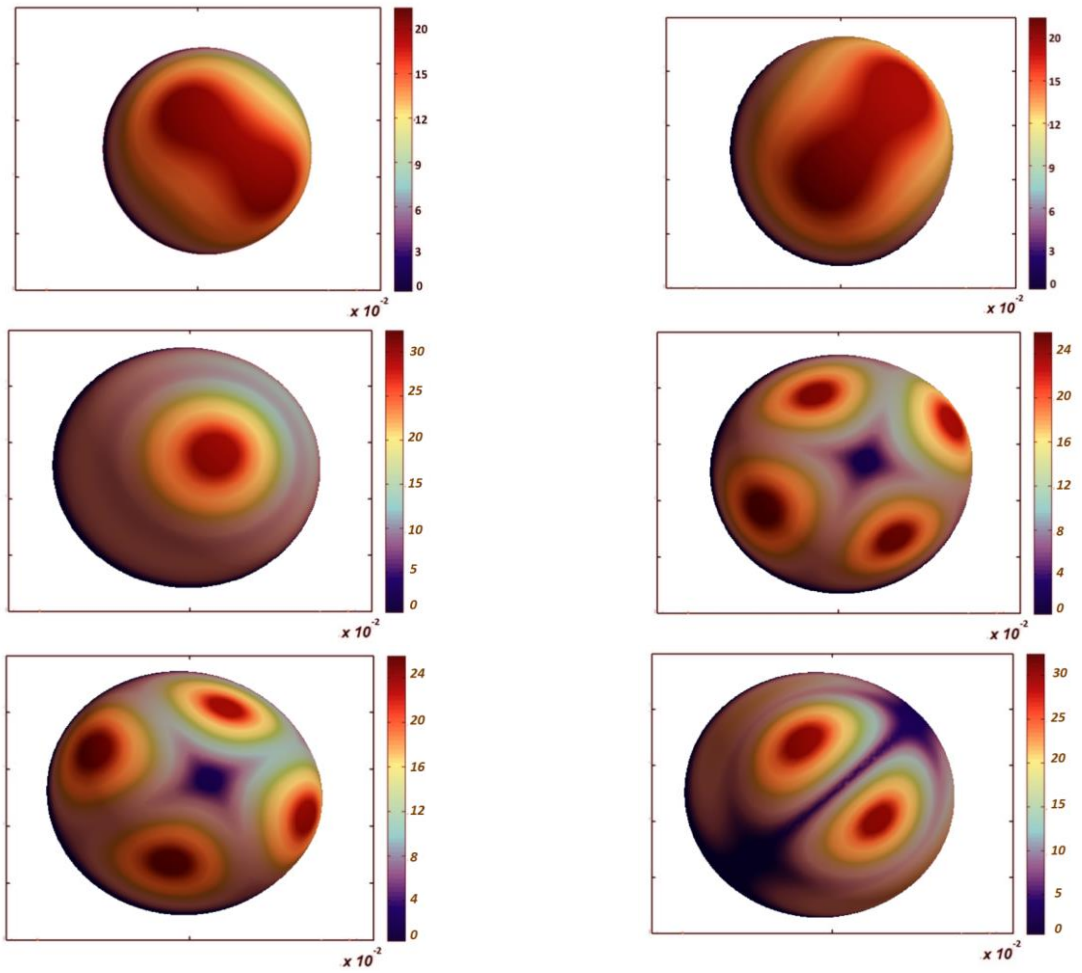

Fig. 3 The first six mode shapes of FG porous spherical cap reinforced by GPLs (θ=180˚, φ=180˚, GPL- X, PD1, e_0=0.4,$\gamma = 0.01wt\%$)

Table 4 Natural frequencies (Hz) of FG-GPL porous spherical cap for various polar angles and GPL patterns (PD2, e_0=0.4,$\gamma = 0.01wt\%$)

GPL pattern	φ	ω_1	ω_2	ω_3	ω_4	ω_5	ω_6
GPL-X	180^0	2069.2	2073.8	2950	3413.8	3422	3904.6
	90^0	3566.1	3920.7	3959.3	4879.2	4948.5	5053.5
GPL-A	180^0	1506	1511.9	2141.2	2473.9	2483.7	2813
	90^0	2563.1	2774.2	2832	3477	3505.9	3557.7
GPL-V	180^0	1335.6	1339.9	1896.9	2190	2197.2	2486.3
	90^0	2272.9	2457	2507.6	3074.6	3100.2	3141.7
GPL-O	180^0	1473.7	1476.9	2080.2	2396.7	2402.2	2696
	90^0	2487.9	2645.3	2719.6	3282.2	3328.5	3354.9
GPL-UD	180^0	1461.2	1480	2114.5	2464.2	2494.9	2849.6
	90^0	2486.2	2714.1	2795.6	3460.8	3520.6	3601.1

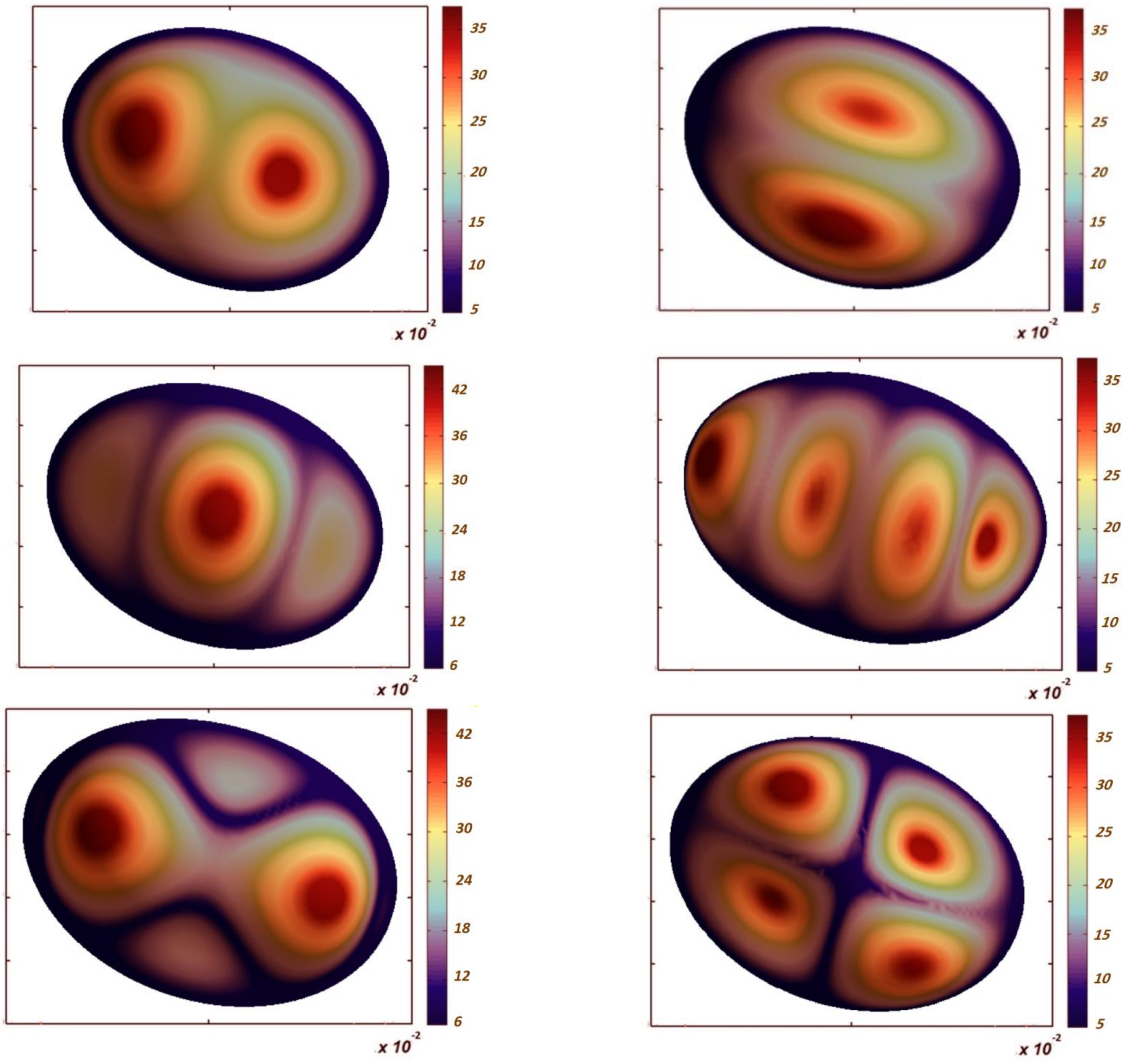

Fig. 4 The first six mode shapes of FG porous spherical cap reinforced by GPLs (θ=180˚, φ=90˚ GPL- X, PD1, e_0=0.4,$\gamma = 0.01wt\%$)

minimum stiffness of the spherical shell. It is mentioned that the difference between maximum and minimum fundamental natural frequency for different porosity distributions is approximately 10%. It means that the porosity distribution does not considerably effect on the natural frequencies of FG-GPL porous spherical cap. The

Table 5 Natural frequencies (Hz) of FG-GPL porous spherical cap for various polar angles and GPL patterns (PD3, e_0=0.4,$\gamma = 0.01wt\%$)

GPL pattern	φ	ω_1	ω_2	ω_3	ω_4	ω_5	ω_6
GPL-X	180^0	2150.2	2154.8	3065.1	3546.7	3554.9	4055.9
	90^0	3705.8	4074	4113.7	5069.1	5140.6	5249.4
GPL-A	180^0	2114.1	2121.2	3018	3494.2	3506.2	4000.3
	90^0	3636.7	3994.3	4042.3	4986.9	5052.6	5164
GPL-V	180^0	1994.7	2001.3	2889	3328.7	3390.1	3884.1
	90^0	3400.2	3794	3860.4	4820	4899.3	5000
GPL-O	180^0	2111.5	2125.3	3020.9	3488.7	3480.1	3976
	90^0	3653.2	4000.8	4050.2	4980.6	5013.1	5100.1
GPL-UD	180^0	2020.7	2001.2	2899.1	3313.2	3389	3800.1
	90^0	3440.4	3800.1	3884.3	4801.4	3977.5	5000

Table 6 Natural frequencies (Hz) of FG-GPL porous spherical cap for various polar angle and porosity distribution (GPLX, e_0=0.2,$\gamma = 0.01wt\%$)

Porosity distribution	φ	ω_1	ω_2	ω_3	ω_4	ω_5	ω_6
PD1	180^0	2001.5	2001.7	2836.1	3271.8	3272.5	3715.9
	90^0	3435.9	3750.9	3789.0	4658.2	4690.4	4774.7
PD2	180^0	1826.3	1826.8	2567.3	2953.2	2954.0	3309.7
	90^0	3083.6	3272.6	3357.7	4045.9	4094.1	4118.6
PD3	180^0	1911.9	1912.2	2711.4	3128.8	3129.5	3558.9
	90^0	3288.6	3601.6	3631.9	4466.5	4511.3	4596.8

Table 7 Natural frequencies **(**Hz**)** of FG-GPL porous spherical cap for various polar angle and weight fraction of GPL Nano-fillers (PD3, e_0=0.5, GPLX)

Weight fraction of Nano-fillers (%wt)	φ	ω_1	ω_2	ω_3	ω_4	ω_5	ω_6
0%	180^0	1477.3	1477.4	2093.4	2413.8	2414.4	2742.0
	90^0	2534.9	2768.8	2796.0	3438.0	3462.6	3527.1
0.5%	180^0	1810.7	1810.8	2572.2	2971.5	2972.1	3385.6
	90^0	3124.9	3430.9	3456.2	4249.4	4304.5	4386.3
1%	180^0	2157.3	2157.5	3059.7	3531.0	3531.7	4016.4
	90^0	3711	4062.6	4098.1	5039.4	5089.3	5184.8

Table 8 Natural frequencies **(**Hz**)** of FG-GPL porous spherical cap for various polar angle and weight fraction of GPL Nano-fillers (PD3, e_0=0.5, GPLA)

Weight fraction of Nano-fillers (%wt)	φ	ω_1	ω_2	ω_3	ω_4	ω_5	ω_6
0%	180^0	1477.3	1477.4	2093.4	2413.8	2414.4	2742
	90^0	2534.9	2768.8	2796	3438	3462.6	3527.1
0.5%	180^0	1756.3	1761.9	2510.4	2909	2918.6	3334.8
	90^0	3031.1	3338.2	3373.2	4160.1	4227	4320.5
1%	180^0	2128.3	2131.4	3030	3496.9	3500	3980.5
	90^0	3664.2	4014.8	4067.3	4983	5022.6	5144

influences of two polar angles and weight fraction of Nano-fillers on the natural frequencies of FG-GPL porous spherical shell (PD3, e_0=0.4, GPLX) are given in Table 7. By increasing the weight fraction of GPLs, the natural frequency of shell considerably increases (approximately 50%), while the mass of structure changes a bit and this

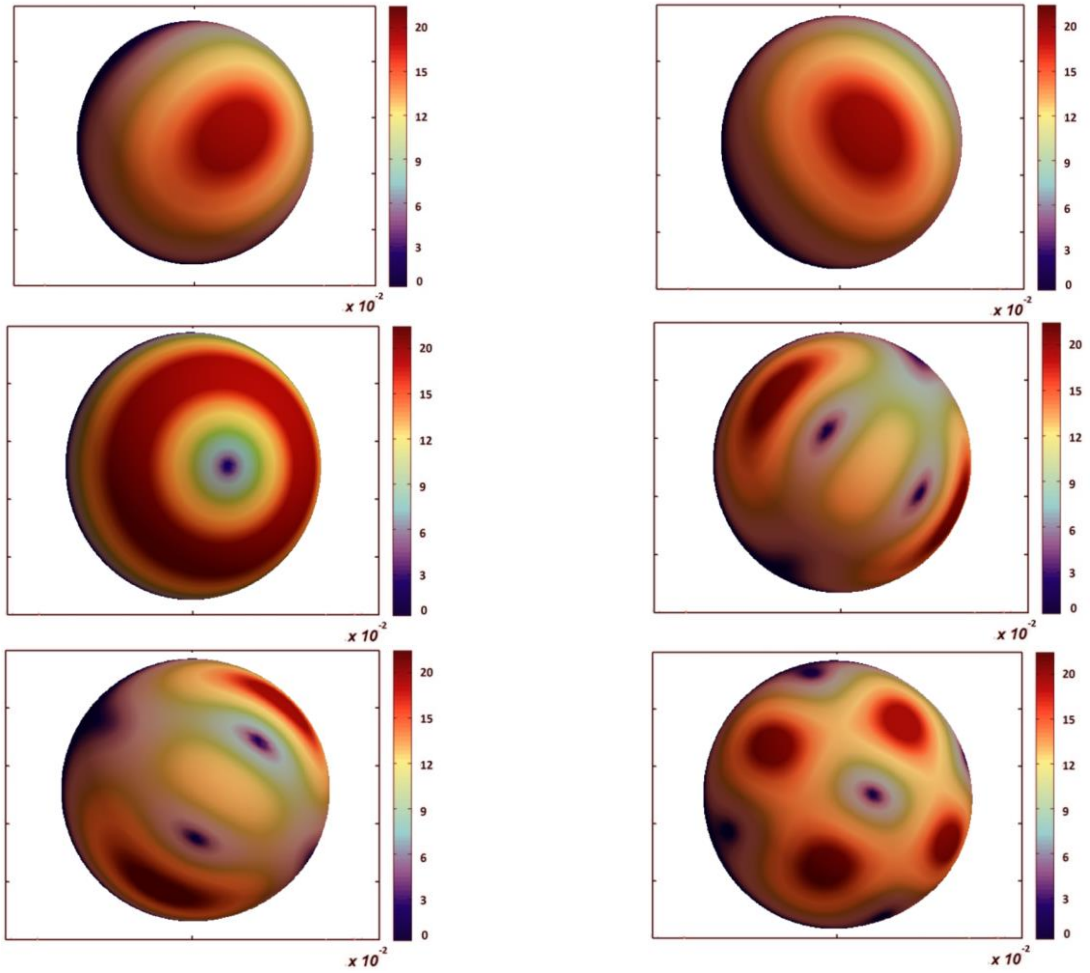

Fig. 5 The first six mode shapes of FG porous spherical cap reinforced by GPLs (θ=180˚, φ=180˚, GPL- X, PD1, e0=0.4, $\gamma = 0.01wt\%$, $K_w = 1 * 10^{12}$)

Table 9 Natural frequencies **(**Hz**)** of FG-GPL porous spherical cap for various polar angle and weight fraction of GPL Nano-fillers (PD3, e_0=0.5, GPLV)

Weight fraction of Nano-fillers (%wt)	φ	ω_1	ω_2	ω_3	ω_4	ω_5	ω_6
0%	1477.3	1477.4	2093.4	2413.8	2414.4	2742	1477.3
	2534.9	2768.8	2796	3438	3462.6	3527.1	2534.9
0.5%	1774.4	1780	2536.1	2938.8	2948.3	3368.6	1774.4
	3062.4	3372.5	3407.8	4202.6	4270	4364.3	3062.4
1%	2135.7	2138	3035.2	3506.2	3510.5	3996.3	2135.7
	3673.8	4026	4065.3	5004.1	5058.7	5158.8	3673.8

Table 10 Natural frequencies **(**Hz**)** of FG-GPL porous spherical cap for various polar angle and weight fraction of GPL Nano-fillers (PD3, e_0=0.5, GPLUD)

Weight fraction of Nano-fillers (%wt)	φ	ω_1	ω_2	ω_3	ω_4	ω_5	ω_6
0%	1477.3	1477.3	1477.4	2093.4	2413.8	2414.4	2742
	2534.9	2534.9	2768.8	2796	3438	3462.6	3527.1
0.5%	1774.4	1557.2	1571.7	2253.2	2626.8	2651.1	3047.
	3062.4	2687.4	2978	3027.6	3756.4	3839.6	3947.6
1%	2135.7	2027.8	2040.9	2912.8	3382.6	3404.5	3895.9
	3673.8	3488.3	3843.2	3901.3	4827.7	4906.	5029.2

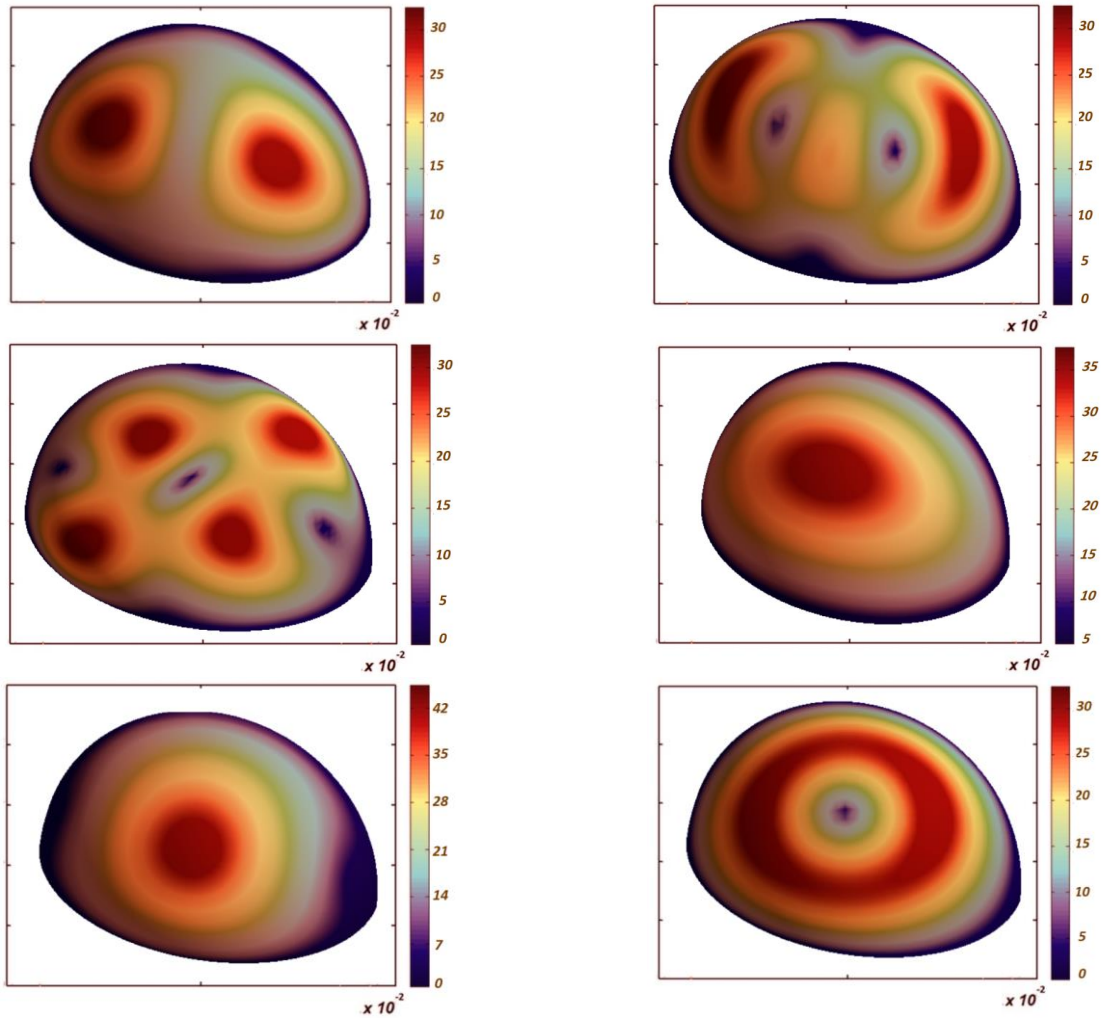

Fig. 6 The first six mode shapes of FG porous spherical cap reinforced by GPLs (θ=180˚, φ=90˚, GPL- X, PD1, e_0=0.4,$\gamma = 0.01wt\%, K_w = 1 * 10^{12}$)

Table 11 Natural frequencies **(**Hz**)** of FG-GPL porous spherical cap for various polar angle and weight fraction of GPL Nano-fillers (PD3, e_0=0.5, GPLO)

Weight fraction of Nano-fillers (%wt)	φ	ω_1	ω_2	ω_3	ω_4	ω_5	ω_6
0%	1477.3	1477.3	1477.4	2093.4	2413.8	2414.4	2742
	2534.9	2534.9	2768.8	2796	3438	3462.6	3527.1
0.5%	1774.4	1611.5	1622.4	2320.1	2698.1	2716.4	3114.7
	3062.4	2781.1	3074.08	3117.4	3858.4	3934.3	4035.3
1%	2135.7	2145.5	2155.6	3049.9	3510.7	3515.3	4005.5
	3673.8	3683.5	4050.2	4080.8	4999.6	5063.7	5174.1

issue can be helpful for aerospace structures where the high stiffness and low density is so important. The same results and conclusions are obtained and shown in Tables 8-11 for GPLV, A, UD and O respectively (PD3, e_0=0.5). Table 12 shows the effect of porosity coefficient on the natural frequencies of FG-GPL porous spherical shell (PD3,$\gamma = 0.01wt\%$,GPLX). When the porosity of the structure increases, both the stiffness and mass of the shell decrease, but the rate of reduction in the mass of the shell is more than its stiffness. Hence, the fundamental natural frequencies of FG–GPL porous spherical shell increase. Comparison between Tables 3-12 denotes that the influence of the porosity coefficient on the natural frequencies is lower than GPL pattern and weight fraction of Nano-filler (its impact is approximately 5%). On the other hand, the effect of GPL pattern, porosity distribution and weight fraction of Nano-fillers on the natural frequencies of FG – GPL porous spherical shell is more than the porosity

Table 12 Natural frequencies (Hz) of FG-GPL porous spherical cap for various polar angle and porosity coefficients (PD3,$\gamma = 0.01wt\%$,GPLX)

e_0	φ	ω_1	ω_2	ω_3	ω_4	ω_5	ω_6
0.2	180^0	1911.9	1912.2	2711.4	3128.8	3129.5	3558.9
	90^0	3288.6	3601.6	3631.9	4466.5	4511.3	4596.8
0.4	180^0	2150.2	2154.8	3065.1	3546.7	3554.9	4055.9
	90^0	3705.8	4074	4113.7	5069.1	5140.6	5249.4
0.5	180^0	2157.3	2157.5	3059.7	3531.0	3531.7	4016.4
	90^0	3711	4062.6	4098.1	5039.4	5089.3	5184.8

Table 13 Natural frequencies of FG-GPL porous spherical cap for different Winkler stiffness coefficient (PD3, $\gamma = 0.01wt\%$,GPLX, e_0=0.2)

Kw($N_{/m}^3$)	ω_1	ω_2	ω_3	ω_4	ω_5	ω_6
1e12	3621.3	3621.5	3780.7	6081.7	6081.7	6468.5
1e11	2813.6	2813.7	3777.9	4273.9	4638.8	4639.5
1e10	2062.4	2062.6	2918.4	3223.4	3224.8	3731.5

coefficient. The first six mode shapes of clamped spherical caps without elastic foundation with θ=180˚, φ=180˚ and also for a spherical cap with θ=180˚, φ=90 are shown in Fig. 3 and Fig. 4, respectively.

The effects of different stiffness coefficients of Winkler elastic foundation on the natural frequencies and mode shapes of spherical cap is shown in Table 13 and Fig. 5 and Fig. 6, respectively. By increasing the Winkler stiffness coefficient, the natural frequencies of structures considerably increase. The first six mode shapes of clamped spherical caps resting on elastic foundation with Kw=1×10^{12} N/m^3 θ=180˚, φ=180˚ and also for a spherical cap with θ=180˚, φ=90 are shown in Fig. 5 and Fig. 6, respectively.

4. Conclusions

Natural frequencies of FG porous spherical cap reinforced by graphene platelet resting on Winkler elastic foundation have been surveyed for the first time. Three different porosity distributions and five GPL patterns are considered along with the shell thickness of the structure. Based on 3D elasticity theory and by employing FEM based on Hamilton principle and Rayleigh- Ritz method, the governing equations of the structure are obtained and solved. The influences of GPL pattern, weight fraction of nanofillers, porosity coefficient, porosity distribution, polar angle and different stiffness of elastic foundation on the natural frequencies of FG-GPL porous spherical cap have been studied. Remarkable findings are as the following:

a) Maximum and minimum natural frequencies are related to GPL-X and GPL-V, respectively.

b) The natural frequencies for GPL-O, A and GPL-UD are almost the same.

c) The maximum and minimum fundamental natural frequencies for FG-X belong to PD1 and PD2, respectively. But, for other distributions of GPLs, it belongs to PD3 and PD2, respectively.

d) By increasing the weight fraction of GPLs, the natural frequencies of the structure considerably increase (approximately 50%).

e) By increasing the porosity of the structure, the fundamental natural frequencies of the structure increase.

f) The influence of porosity coefficient on the natural frequencies is lower than the weight fraction of Nano-filler (its impact is approximately 5%)

References

Akbaş, Ş.D. (2021), "Dynamic analysis of axially functionally graded porous beams under a moving load", *Steel Compos. Struct.*, **39**(6), 811-821. https://doi.org/10.12989/scs.2021.39.6.811

Al-Furjan, M.S.H., Habibi, M., Ghabussi, A., Safarpour, H., Safarpour, M. and Tounsi, A. (2021), "Non-polynomial frame-work for stress and strain response of the FG-GPLRC disk using three-dimensional refined higher-order theory", *Eng. Struct.*, **228**, 111496. https://doi.org/10.1016/j.engstruct.2020.111496

Al-Furjan, M.S.H., Habibi, M., Ni, J., Jung, D.W. and Tounsi, A. (2022a), "Frequency simulation of viscoelastic multi-phase reinforced fully symmetric systems", *Eng. Comput.*, **38**(Suppl 5), 3725-3741. https://doi.org/10.1007/s00366-020-01200-x

Al-Furjan, M.S.H., Habibi, M., Jung, D.W., Sadeghi, S., Safarpour, H., Tounsi, A. and Chen, G. (2022b), "A computational framework for propagated waves in a sandwich doubly curved nanocomposite panel", *Eng. Comput.*, **38**(2), 1679-1696. https://doi.org/10.1007/s00366-020-01130-8

Al-Osta, M.A., Saidi, H., Tounsi, A., Al-Dulaijan, S.U., Al-Zahrani, M.M., Sharif, A. and Tounsi, A. (2021), "Influence of porosity on the hygro-thermo-mechanical bending response of an AFG ceramic-metal plates using an integral plate model", *Smart Struct. Syst.*, **28**(4), 499-513. https://doi.org/10.12989/sss.2021.28.4.499

Ansari, R., Hassani, R., Gholami, R. and Rouhi, H. (2021), "Buckling and postbuckling of plates made of FG-GPL-

reinforced porous nanocomposite with various shapes and boundary conditions", *Int. J. Struct. Stabil. Dyn.*, **21**(5), 2150063. https://doi.org/10.1142/S0219455421500632

Arshid, E., Khorasani, M., Soleimani-Javid, Z., Amir, S. and Tounsi, A. (2021), "Porosity-dependent vibration analysis of FG microplates embedded by polymeric nanocomposite patches considering hygrothermal effect via an innovative plate theory", *Eng. Comput.*, 1-22. https://doi.org/10.1007/s00366-021-01382-y

Artioli, E. and Viola, E. (2006), "Free vibration analysis of spherical caps using a GDQ numerical solution", *J. Press. Vessel Technol.*, **128**(3), 370-378. https://doi.org/10.1115/1.2217970

Asadzadeh, Z. and Eslami, M.R. (2018), "Nonlinear axisymmetric, thermally induced vibrations of a functionally graded spherical cap", *J. Mech. Eng. Transact. ISME*, **20**(3), 133-169.

Babaei, M., Kiarasi, F., Hossaeini Marashi, S.M., Ebadati, M., Masoumi, F. and Asemi, K. (2021), "Stress wave propagation and natural frequency analysis of functionally graded graphene platelet-reinforced porous joined conical–cylindrical–conical shell", *Waves Random Complex Media*, 1-33. https://doi.org/10.1080/17455030.2021.2003478

Bahaadini, R., Saidi, A.R., Arabjamaloei, Z. and Ghanbari-Nejad-Parizi, A. (2019), "Vibration analysis of functionally graded graphene reinforced porous nanocomposite shells", *Int. J. Appl. Mech.*, **11**(7), 1950068. https://doi.org/10.1142/S1758825119500686

Barzegar, A.R. and Fadaee, M. (2018), "Thermal vibration analysis of functionally graded shallow spherical caps by introducing a decoupling analytical approach", *Appl. Math. Modell.*, **58**, 473-486. https://doi.org/10.1016/j.apm.2018.02.018

Bekkaye, T.H.L., Fahsi, B., Bousahla, A.A., Bourada, F., Tounsi, A., Benrahou, K.H. and Al-Zahrani, M.M. (2020), "Porosity-dependent mechanical behaviors of FG plate using refined trigonometric shear deformation theory", *Comput. Concr.*, **26**(5), 439-450. http://doi.org/10.12989/cac.2020.26.5.439

Bellifa, H., Chikh, A., Bousahla, A.A., Bourada, F., Tounsi, A., Benrahou, K. H. and Tounsi, A. (2021), "Influence of porosity on thermal buckling behavior of functionally graded beams", *Smart Struct. Syst.*, **27**(4), 719-728. https://doi.org/10.12989/sss.2021.27.4.719

Bouafia, H., Chikh, A., Bousahla, A.A., Bourada, F., Heireche, H., Tounsi, A. and Hussain, M. (2021), "Natural frequencies of FGM nanoplates embedded in an elastic medium", *Adv. Nano Res.*, **11**(3), 239-249. http://doi.org/10.12989/anr.2021.11.3.239

Bot, I.K., Bousahla, A.A., Zemri, A., Sekkal, M., Kaci, A., Bourada, F. and Mahmoud, S.R. (2022), "Effects of Pasternak foundation on the bending behavior of FG porous plates in hygrothermal environment", *Steel Compos. Struct.*, **43**(6), 821-837. https://doi.org/10.12989/scs.2022.43.6.821

Cuong-Le, T., Nguyen, K. D., Le-Minh, H., Phan-Vu, P., Nguyen-Trong, P. and Tounsi, A. (2022), "Nonlinear bending analysis of porous sigmoid FGM nanoplate via IGA and nonlocal strain gradient theory", *Adv. Nano Res.*, **12**(5), 441. https://doi.org/10.12989/anr.2022.12.5.441

Du, Y., Huo, R., Pang, F., Li, S., Huang, Y. and Zhang, H (2019), "Free vibration of spherical cap subjected to various boundary conditions", *Adv. Mech. Eng.*, **11**(9), 1687814019879261. https://doi.org/10.1177/1687814019879261

Du, Y., Sun, L., Miao, X., Pang, F., Li, H. and Wang, S. (2019), "A unified formulation for free vibration of spherical cap based on the Ritz method", *Shock Vib.*, 18. https://doi.org/10.1155/2019/7470460

Ebrahimi, F., Seyfi, A., Dabbagh, A. and Tornabene, F. (2019), "Wave dispersion characteristics of porous graphene platelet-reinforced composite shells", *Struct. Eng. Mech.*, **71**(1), 99-107. https://doi.org/10.12989/sem.2019.71.1.099

Faghidian, S.A. and Tounsi, A. (2022), "Dynamic characteristics of mixture unified gradient elastic nanobeams", *Facta Universitatis, Series Mech. Eng.*, **20**(3), 539-552. https://doi.org/10.22190/FUME220703035F

Flis, J. and Muc, A. (2021), "Influence of coupling effects on analytical solutions of functionally graded (FG) spherical shells of revolution", *Rev. Adv. Mater. Sci.*, **60**(1), 761-770. https://doi.org/10.1515/rams-2021-0064

Gao, C., Pang, F., Li, H. and Li, L. (2020), "An approximate solution for vibrations of uniform and stepped functionally graded spherical cap based on Ritz method", *Compos. Struct.*, **233**, 111640. https://doi.org/10.1016/j.compstruct.2019.111640

Gautham, B.P. and Ganesan, N. (1992), "Free vibration analysis of thick spherical shells", *Comput. Struct.*, **45**(2), 307-313. https://doi.org/10.1016/0045-7949(92)90414-U

Guellil, M., Saidi, H., Bourada, F., Bousahla, A.A., Tounsi, A., Al-Zahrani, M.M. and Mahmoud, S.R. (2021), "Influences of porosity distributions and boundary conditions on mechanical bending response of functionally graded plates resting on Pasternak foundation", *Steel Compos. Struct.*, **38**(1), 1. https://doi.org/10.12989/scs.2021.38.1.001

Hadji, M., Bouhadra, A., Mamen, B., Menasria, A., Bousahla, A.A., Bourada, F., Bourada, M., Benrahou, K.H., Tounsi, A. (2023), "Combined influence of porosity and elastic foundation parameters on the bending behavior of advanced sandwich structures", *Steel Compos. Struct.*, **46**(1), 1-13. https://doi.org/10.12989/scs.2023.46.1.001

Heidari, F., Taheri, K., Sheybani, M., Janghorban, M. and Tounsi, A. (2021), "On the mechanics of nanocomposites reinforced by wavy/defected/aggregated nanotubes", *Steel Compos. Struct.*, **38**(5), 533-545. http://doi.org/10.12989/scs.2021.38.5.533

Huang, Y., Karami, B., Shahsavari, D. and Tounsi, A. (2021), "Static stability analysis of carbon nanotube reinforced polymeric composite doubly curved micro-shell panels", *Arch. Civil Mech. Eng.*, **21**(4), 139. https://doi.org/10.1007/s43452-021-00291-7

Katiyar, V., Gupta, A. and Tounsi, A. (2022), "Microstructural/ geometric imperfection sensitivity on the vibration response of geometrically discontinuous bi-directional functionally graded plates (2D-FGPs) with partial supports by using FEM", *Steel Compos. Struct.*, **45**(5), 621-640. https://doi.org/10.12989/scs.2022.45.5.621

Khinchi, A. and Sharma, P, (2020), "Free vibration analysis of isotropic spherical cap and FG-spherical cap with cut-out using COMSOL", *AIP Conference Proceedings*, **2220**(1), 130074. https://doi.org/10.1063/5.0001299

Khinchi, A. and Sharma, P. (2019), "Review on vibration analysis of functionally graded material (FGM) spherical shell", *14th ICRTESM*, 96-101.

Kiarasi, F., Babaei, M., Mollaei, S., Mohammadi, M. and Asemi, K. (2021), "Free vibration analysis of FG porous joined truncated conical-cylindrical shell reinforced by graphene platelets", *Adv. Nano Res.*, **11**(4), 361-380. https://doi.org/10.12989/anr.2021.11.4.361

Kitipornchai, S., Chen, D., and Yang, J. (2017), "Free vibration and elastic buckling of functionally graded porous beams reinforced by graphene platelets", *Mater. Des.*, **116**, 656-665. https://doi.org/10.1016/j.matdes.2016.12.061

Kong, F., Dong, F., Duan, M., Habibi, M., Safarpour, H. and Tounsi, A. (2022), "On the vibrations of the Electrorheological sandwich disk with composite face sheets considering pre and post-yield regions", *Thin Wall. Struct.*, **179**, 109631. https://doi.org/10.1016/j.tws.2022.109631

Kumar, Y., Gupta, A. and Tounsi, A. (2021), "Size-dependent vibration response of porous graded nanostructure with FEM

and nonlocal continuum model", *Adv. Nano Res.*, **11**(1), 1. http://doi.org/10.12989/anr.2021.11.1.001

Li, H., Pang, F., Ren, Y., Miao, X. and Ye, K. (2019), "Free vibration characteristics of functionally graded porous spherical shell with general boundary conditions by using first-order shear deformation theory", *Thin Wall. Struct.*, **144**, 106331. https://doi.org/10.1016/j.tws.2019.106331

Liu, G., Wu, S., Shahsavari, D., Karami, B. and Tounsi, A. (2022), "Dynamics of imperfect inhomogeneous nanoplate with exponentially-varying properties resting on viscoelastic foundation", *Eur. J. Mech. A Solids*, **95**, 104649. https://doi.org/10.1016/j.euromechsol.2022.104649

Madenci, E. and Özkılıç, Y.O. (2021), "Free vibration analysis of open-cell FG porous beams: Analytical, numerical and ANN approaches", *Steel Compos. Struct.*, **40**(2), 157-173. https://doi.org/10.12989/scs.2021.40.2.157

Mangalasseri, A.S., Mahesh, V., Mukunda, S., Mahesh, V., Ponnusami, S.A., Harursampath, D., Tounsi, A. (2023), "Vibration based energy harvesting performance of magneto-electro-elastic beams reinforced with carbon nanotubes", *Adv. Nano Res.*, **14**(1), 27-43. https://doi.org/10.12989/anr.2023.14.1.027

Minh, T.Q., Dong, D.T., Duc, V.M., Tien, N.V., Phuong, N.T. and Nam, V.H. (2022), "Nonlinear axisymmetric vibration of sandwich FGM shallow spherical caps with lightweight porous core", *In CIGOS 2021, Emerging Technologies and Applications for Green Infrastructure*, Springer, Singapore, **203**, 381-389. https://doi.org/10.1007/978-981-16-7160-9_38

Mirjavadi, S.S., Forsat, M., Barati, M.R. and Hamouda, A.S. (2021), "Geometrically nonlinear vibration analysis of eccentrically stiffened porous functionally graded annular spherical shell segments", *Mech. Based Des. Struct.*, **50**(6), 1-15. https://doi.org/10.1080/15397734.2020.1771729

Moradi-Dastjerdi, R. and Behdinan, K. (2021), "Stress waves in thick porous graphene-reinforced cylinders under thermal gradient environments", *Aerosp. Sci. Technol.*, **110**, 106476. https://doi.org/10.1016/j.ast.2020.106476

Nejadi, M.M., Mohammadimehr, M. and Mehrabi, M. (2021), "Free vibration and stability analysis of sandwich pipe by considering porosity and graphene platelet effects on conveying fluid flow", *Alexandria Eng. J.*, **60**(1), 1945-1954. https://doi.org/10.1016/j.aej.2020.11.042

Nguyen, Q.H., Nguyen, L.B., Nguyen, H.B. and Nguyen-Xuan, H. (2020), "A three-variable high order shear deformation theory for isogeometric free vibration, buckling and instability analysis of FG porous plates reinforced by graphene platelets", *Compos. Struct.*, **245**, 112321. https://doi.org/10.1016/j.compstruct.2020.112321

Pang, F., Gao, C., Cui, J., Ren, Y., Li, H. and Wang, H. (2019), "A semianalytical approach for free vibration characteristics of functionally graded spherical shell based on first-order shear deformation theory", *Shock Vib.*, **2019**, 18. https://doi.org/10.1155/2019/7352901

Pourjabari, A., Hajilak, Z.E., Mohammadi, A., Habibi, M. and Safarpour, H. (2019), "Effect of porosity on free and forced vibration characteristics of the GPL reinforcement composite nanostructures", *Comput. Math. Appl.*, **77**(10), 2608-2626. https://doi.org/10.1016/j.camwa.2018.12.041

Prakash, T., Singh, M.K. and Ganapathi, M. (2006), "Vibrations and thermal stability of functionally graded spherical caps", *Struct. Eng. Mech.*, **24**(4), 447-461. https://doi.org/10.12989/sem.2006.24.4.447

Punera, D. and Kant, T. (2019), "A critical review of stress and vibration analyses of functionally graded shell structures", *Compos. Struct.*, **210**, 787-809. https://doi.org/10.1016/j.compstruct.2018.11.084

Ram, K.S. and Babu, T.S. (2002), "Free vibration of composite spherical shell cap with and without a cutout", *Comput. Struct.*, **80**(23), 1749-1756. https://doi.org/10.1016/S0045-949(02)00210-9

Rouabhia, A., Chikh, A., Bousahla, A.A., Bourada, F., Heireche, H., Tounsi, A. and Structures, C. (2020), "Physical stability response of a SLGS resting on viscoelastic medium using nonlocal integral first-order theory", *Steel Compos. Struct.*, **37**(6), 695-709. https://doi.org/10.12989/scs.2020.37.6.695

Sadd, M.H. (2009). Elasticity: theory, applications, and numerics. Academic Press.

Safarpour, M., Rahimi, A. and Alibeigloo, A. (2020), "Static and free vibration analysis of graphene platelets reinforced composite truncated conical shell, cylindrical shell, and annular plate using theory of elasticity and DQM", *Mech. Based Des. Struct.*, **48**(4) 496-524. https://doi.org/10.1016/j.compstruct.2018.03.090

Salehi, M., Gholami, R. and Ansari, R. (2021), "Analytical solution approach for nonlinear vibration of shear deformable imperfect FG-GPLR porous nanocomposite cylindrical shells", *Mech. Based Des. Struct.*, 1-23. https://doi.org/10.1080/15397734.2021.1891096

She, G.L., Liu, H.B. and Karami, B. (2020), "On resonance behavior of porous FG curved nanobeams", *Steel Compos. Struct.*, **36**(2), 179-186. https://doi.org/10.12989/scs.2020.36.2.179

Su, Z., Jin, G., Shi, S. and Ye, T. (2014), "A unified accurate solution for vibration analysis of arbitrary functionally graded spherical shell segments with general end restraints", *Compos. Struct.*, **111**, 271-284. https://doi.org/10.1016/j.compstruct.2014.01.006

Susmith, A.V. and Ram, K.S. (2019), "Free vibration of functionally graded carbon nanotube reinforced composite spherical shell cap", *AIP Conf Proc.*, **2200**(1), 020040. https://doi.org/10.1063/1.5141210

Tao, C. and Dai, T. (2021), "Isogeometric analysis for postbuckling of sandwich cylindrical shell panels with graphene platelet reinforced functionally graded porous core", *Compos. Struct.*, **260**, 113258. https://doi.org/10.1016/j.compstruct.2020.113258

Thi Phuong, N., Hoai Nam, V. and Thuy Dong, D. (2020), "Nonlinear vibration of functionally graded sandwich shallow spherical caps resting on elastic foundations by using first-order shear deformation theory in thermal environment", *J. Sandw. Struct. Mater.*, **22**(4), 1157-1183. https://doi.org/10.1177/1099636218782 64

Ton-That, H.L., Nguyen-Van, H. and Chau-Dinh, T. (2021), "A novel quadrilateral element for analysis of functionally graded porous plates/shells reinforced by graphene platelets", *Arch. Appl. Mech.*, **91**(6), 2435-2466. https://doi.org/10.1007/s00419-021-01893-6

Van Vinh, P. and Tounsi, A. (2022a), "The role of spatial variation of the nonlocal parameter on the free vibration of functionally graded sandwich nanoplates", *Eng. Comput.*, **38**(Suppl 5), 4301-4319. https://doi.org/10.1007/s00366-021-01475-8

Van Vinh, P. and Tounsi, A. (2022b), "Free vibration analysis of functionally graded doubly curved nanoshells using nonlocal first-order shear deformation theory with variable nonlocal parameters", *Thin Wall. Struct.*, **174**, 109084. https://doi.org/10.1016/j.tws.2022.109084

Van Vinh, P., Van Chinh, N. and Tounsi, A. (2022), "Static bending and buckling analysis of bi-directional functionally graded porous plates using an improved first-order shear deformation theory and FEM", *Eur. J. Mech A Solids*, **96**, 104743. https://doi.org/10.1016/j.euromechsol.2022.104743

Wang, Y.Q., Ye, C. and Zu, J.W. (2019), "Nonlinear vibration of metal foam cylindrical shells reinforced with graphene platelets", *Aerosp. Sci. Technol.*, **85**, 359-370.

https://doi.org/10.1016/j.ast.2018.12.022

Yaghoobi, H. and Taheri, F. (2020), "Analytical solution and statistical analysis of buckling capacity of sandwich plates with uniform and non-uniform porous core reinforced with graphene nanoplatelets", *Composite Structures*., **252**, 112700. https://doi.org/10.1016/j.compstruct.2020.112700

Yang, J., Chen, D. and Kitipornchai, S. (2018), "Buckling and free vibration analyses of functionally graded graphene reinforced porous nanocomposite plates based on Chebyshev-Ritz method", *Compos. Struct*., **193**, 281-294. https://doi.org/10.1016/j.compstruct.2018.03.090

Ye, C. and Wang, Y.Q. (2021), "Nonlinear forced vibration of functionally graded graphene platelet-reinforced metal foam cylindrical shells: Internal resonances", *Nonlinear Dyn*., **104**(3), 2051-2069. https://doi.org/10.1007/s11071-021-06401-7

Ye, T., Jin, G. and Su, Z. (2014), "Three-dimensional vibration analysis of laminated functionally graded spherical shells with general boundary conditions", *Compos. Struct*., **116**, 571-588. https://doi.org/10.1016/j.compstruct.2014.05.046

Zannon, M., Abu-Rqayiq, A. and Al-bdour, A. (2020), "Free vibration frequency of thick FGM spherical shells based on a third-order shear deformation theory", *Eur. J. Pure Appl. Math*., **13**(4), 766-778. https://doi.org/10.29020/nybg.ejpam.v13i4.3826

Zhou, X., Wang, Y. and Zhang, W. (2021), "Vibration and flutter characteristics of GPL-reinforced functionally graded porous cylindrical panels subjected to supersonic flow", *Acta Astronautica*., **183**, 89-100. https://doi.org/10.1016/j.actaastro.2021.03.003

Zhou, Z., Ni, Y., Tong, Z., Zhu, S., Sun, J. and Xu, X. (2019), "Accurate nonlinear buckling analysis of functionally graded porous graphene platelet reinforced composite cylindrical shells", *Int. J. Mech. Sci*., **151**, 537-550. https://doi.org/10.1016/j.ijmecsci.2018.12.012

CC